RSC Advances

ROYAL SOCIETY OF CHEMISTRY

www.rsc.org/advances

Journal Name

ARTICLE

Electronic structure and optical properties of Fe-doped SnS_2 from first-principle calculations

Received 00th January 2015,
Accepted 00th January 2015

DOI: 10.1039/x0xx00000x

www.rsc.org/

Lili Sun,[a] Wei Zhou,[a] Yanyu Liu,[a] Dandan Yu,[a] Yinghua Liang[b] and Ping Wu*[a]

The electronic structure and optical properties of Fe-doped SnS_2 were investigated using first-principle calculations. The results suggest that Fe-doped SnS_2 is half-metal and the band gap decreases due to the Fe doping, leading to red shift of the absorption edges. The enhancement of the absorption efficiency in the low energy region is also observed. Furthermore, the absorption coefficient in visible region increases monotonically with increasing Fe doping concentrations ($0\% \le x \le 12.5\%$), while the intensity of additional peaks in infrared region increases with small doping concentrations (less than $x = 8.33\%$) and decreases with heavy doping.

1. Introduction

With the irresistible growing global demand for energy, solar energy has been paid a great deal of attention due to its abundant, clean and renewable characteristics. Photovoltaic device is the most important way to make full use of solar energy. Among the current photovoltaic devices, the development and applications of first generation solar cells based on crystalline or amorphous silicon have been limited because of its high cost, complex process of fabrication and low optical absorption coefficient.[1,2] In addition, solar cells based on CdTe and $CuInGaSe_2$ have not been widely used for containing low abundant and expensive elements Te and In.[3-5] Up to now, quite a lot of efforts have been concentrated on searching for new photovoltaic absorber materials based on metal sulfide, such as ZnS, CdS, FeS_2, MoS_2 and SnS_2.[6-11] In this paper, our interest will concentrate on SnS_2 with the advantage of high chemical stabilizations, nontoxicity, low cost and abundance. As an indirect gap semiconductor with a band gap value of ~2.0 eV, SnS_2 can absorb most of the ultraviolet light and a small amount of visible light. Besides, SnS_2 have larger specific surface area than conventional materials due to its hexagonal layered crystalline structure. These excellent characteristics make SnS_2 an intriguing material applied in optoelectronic devices.[12-16]

As is well known, the proportion of visible light in solar energy is around 45%, while the ultraviolet light is only 5%.[17] In addition, great solar cell absorbers should meet the criteria with closing to optimal band gap value around 1.5 eV and high optical absorption coefficient more than 1.0×10^4 cm^{-1}. Therefore, to achieve the goal of SnS_2 as a photovoltaic absorber material, the biggest challenge is to appropriately narrow its optical band gap and reach a much higher absorption coefficient in the whole solar range. More recently, many research works have proved that the impurities and defects indeed have a significant influence on the optoelectronic properties such as strong absorption in the low energy region (including visible and near-infrared light regions) and high-efficient photocatalytic activity in the visible-light region of the SnS_2 host materials.[18-21] For example, Xia *et al*. found that Ti doping into SnS_2 could narrow its band gap and improve its absorption coefficient in the visible-light region.[22] Kiruthigaa *et al*. proved that Zn-doped SnS_2 could be used as photocatalytic materials.[23] In addition, V-doped SnS_2 was investigated as a new intermediate band material to produce an absorption spectrum in the UV-Vis-NIR range.[24,25] These studies suggest that the applications of SnS_2 have a bright future in optoelectronic devices. While the shortage of Ti and Zn doped SnS_2 is that they could not utilize the sunlight in the infrared region. For V-doped SnS_2, the photocatalytic efficiency appeared lower than that of pure SnS_2 as photon energy was higher than the SnS_2 band gap. Thus, in order to utilize the sunlight more effectively, other elements should be considered to dope into the SnS_2 host material.

As is well known, FeS_2 has a band gap of 0.95 eV,[26] and Fe has been successfully used to improve the optical properties of In_2S_3.[27] Besides, few research work has been done on the electronic and optical properties of Fe-doped SnS_2 until now. In this work, the first-principle calculations based on density functional theory (DFT) were performed to systematically study the electronic and optical properties of Fe-doped SnS_2 systems. Meanwhile, five different structure configurations

[a] Department of Applied Physics, Tianjin Key Laboratory of Low Dimensional Materials Physics and Preparing Technology, Faculty of Science, Tianjin University, Tianjin 300072, People's Republic of China.
[b] College of Chemical Engineering, North China University of Science and Technology, Tangshan 063009, People's Republic of China.
* Corresponding author. Tel.: +86 022 27408599.
E-mail address: pingwu@tju.edu.cn (P. Wu).
See DOI: 10.1039/x0xx00000x

corresponding to Fe doping concentrations of x = 0%, 5.56%, 6.25%, 8.33%, 12.50% were adopted to explore the effect of Fe doping concentrations on these properties of SnS_2. The obtained results show that Fe doping into SnS_2 could lead to strong absorption in the full solar spectrum area due to the formation of impurity bands in the band gap, which is similar to the results of Fe-doped In_2S_3. But there is difference between them. The intensity of emerging peaks in infrared region increases monotonically with increasing Fe doping concentrations for Fe-doped In_2S_3,[27] while increases with small doping concentrations (less than x = 8.33%) and decreases with heavy doping for Fe-doped SnS_2. Theoretical study on the electronic and optical properties of SnS_2 host materials is significant for deeper understanding of photoelectric mechanism and better applications of these photovoltaic absorber materials.

2. Methods and computational details

All the calculations carried out using projector augment wave (PAW) pseudopotentials are based on the DFT method, as implemented in the Vienna *ab initio* Simulation Package (VASP).[28] The generalized gradient approximation (GGA) with the Perdew-Burke-Ernzerhof (PBE) formula was adopted for the exchange-correlation potential, plusing the onsite Coulomb interaction U within GGA.[29] A cutoff energy of 400 eV was set for the plane wave expansion, with total energy converging to lower than 5×10^{-6} eV/atom between two steps. Both cell and atoms were fully relaxed until the residual forces were less than 0.01 eV/Å. The valence electron configurations Sn ($4d^{10}5s^25p^2$), Fe ($3d^64s^2$) and S ($3s^23p^4$) were considered in this work. A grid of 7×7×4 k-point was used for the unit cell. While for Fe-doped SnS_2, four different configurations of SnS_2 supercells were considered, which correspond to Fe doping concentrations of x = 5.56%, 6.25%, 8.33% and 12.50%, respectively. Besides, Monkhorst-Pack k-point meshes of 3×3×2, 4×4×1, 4×4×2 and 4×4×3 were used for Brillouin zone sampling.[30] Moreover, the van der Waals interaction was considered by using Grimme's DFT-D2 method due to the characteristic of layer-type lattice.[31] Then all the calculations on electronic and optical properties were performed on the basis of the optimized supercells.

3. Results and discussions

It is noteworthy that the method of GGA usually underestimates the band gap for the static correlation of common approximations and delocalization error.[32] Therefore, for the sake of accurately describing the electronic structure of SnS_2, it is necessary to use other methods to correct the band-gap value. Dudarev *et al*. proved that the method of determining the value of U in relation to single ion could correct the error of GGA.[33] Therefore, U = 1.7 eV and U = 9.0 eV were chosen for Fe-3d and Sn-4d electrons on the basis of calculating the band gap values of FeS_2 and SnS_2.[26,34]

The optimized lattice parameters of pure SnS_2 are a = 3.519 Å and c = 5.839 Å, which are in good agreement with experimental values (a = 3.649 Å, c = 5.899 Å).[35] The calculated band structure and density of states (DOS) of pure SnS_2 are shown in Fig. 1 as a reference. It can be seen from Fig. 1(a) that the valence band maximum (VBM) lies at the Γ point and the conduction band minimum (CBM) locates between M and L points, indicating that pure SnS_2 is an indirect gap semiconductor. The calculated band gap is 1.81 eV, which is close to the experimental value of ~2.00 eV.[16] Moreover, as shown in Fig. 1(b), the conduction band is mainly dominated by the 5s and 5p orbitals of the Sn atom, and the 3p orbitals of the S atom. While the lower valence band from -7 to -5 eV mostly originates from the 5s orbitals of the Sn atom and the 3p orbitals of the S atom, and the upper valence band from -5 to 0 eV is derived from the 3p orbitals of the S atom and a little 5p orbitals of the Sn atom. These properties have a good consistency with the previous results presented by Xia *et al*,[22] which suggests that the results of GGA+U method are reliable.

Table 1 The lattice constants (a and c), and the bond length between the Fe(Sn) atom and its nearest S atoms ($d_{Fe(Sn)-S}$) for pure SnS_2 and Fe-doped SnS_2.

Structural parameters (Å)	0%	5.56%	6.25%	8.33%	12.50%
a	3.519	3.508	3.507	3.505	3.498
c	5.839	5.795	5.793	5.618	5.781
$d_{Fe(Sn)-S}$	2.449	2.360	2.367	2.369	2.365

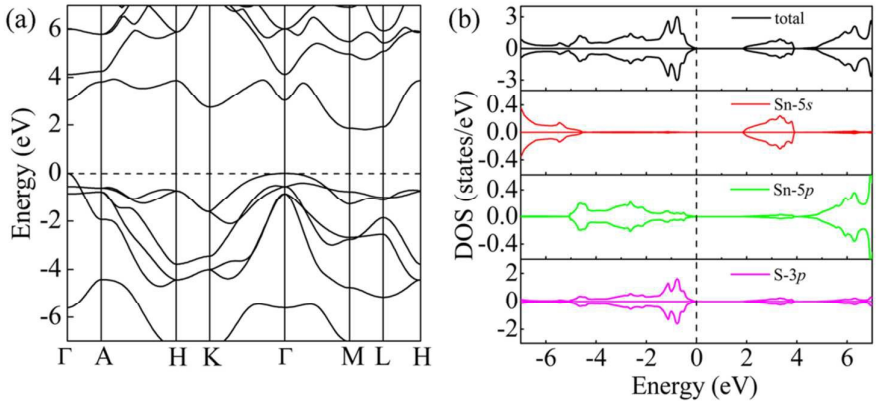

Fig. 1 (a) Band structure and (b) DOS of unit SnS_2. The Fermi level is set to 0.

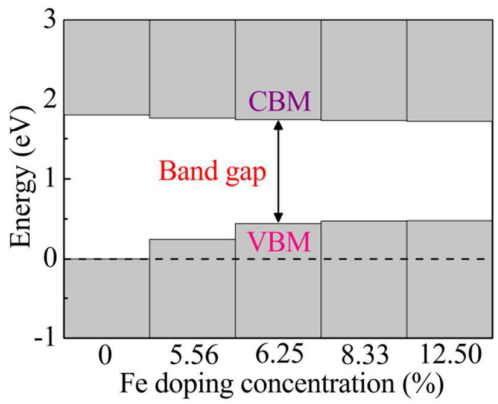

Fig. 2 The band edge of Fe-doped SnS_2 with different doping concentrations of x = 0%, 5.56%, 6.25%, 8.33% and 12.50%.

In order to investigate the effect of Fe doping concentrations on the electronic structure and search the ideal band gap for photovoltaic absorber material based on SnS_2, the structural parameters and band gaps of $Sn_{1-x}Fe_xS_2$ (x = 5.56%, 6.25%, 8.33%, 12.50%) are calculated for substituting one Sn atom with Fe in four different configurations of SnS_2 supercells. It can be seen from Table 1 that the Fe doping leads to the decrease of lattice parameters of SnS_2, which may originate from the difference of bond length between Sn-S and Fe-S. The relaxed bond length of Fe-S is shorter than that of Sn-S. The reason is that the electronegativity difference between Fe and S atoms (0.75) is larger than that between Sn and S atoms (0.62). In addition, the CBM and VBM positions of the SnS_2 systems are aligned with the core energy level of S-2*s* orbitals. For the pure SnS_2, the VBM position locates at the Fermi level. Based on the relative positions as compared with that of pure SnS_2, the band gaps of doped SnS_2 are obtained from the CBM and VBM positions presented in Fig. 2. Obviously, the band gap decreases monotonically with increasing Fe concentrations in the SnS_2 host material, which implies that Fe doping can effectively modify the band gap of SnS_2. One thing should be noticed is that the change trend of band gap is gradually gentle, especially at the doping concentrations of 8.33% to 12.50%.

To specifically analyze the origin of the band gap narrowing of Fe-doped SnS_2, $Sn_{1-x}Fe_xS_2$ (x = 6.25%) is selected as the representative model. Meanwhile, the band structure, total density of states (TDOS) and partial density of states (PDOS) of $Sn_{1-x}Fe_xS_2$ (x = 6.25%) are calculated and illustrated in Fig. 3 and Fig. 4. Compared with undoped SnS_2, the most notable characteristic of the band structure for Fe-doped SnS_2 is that the Fermi level emerges into valence band in the minority spin channel while the majority spin channel shows an appreciable gap. This result demonstrates that the material is half-metal. Meanwhile, as shown in Fig. 4, the 3*p* orbitals of the S atom are the most dominant from -6.00 to -0.21 eV in valence band, while the 5*s* and 5*p* orbitals of the Sn atom mostly locate in the energy range from 1.45 to 3.80 eV and from 4.56 to 7.00 eV, respectively. It can be found that the impurity bands in the band gap are mainly composed of Fe 3*d* states, which are separated into seven bands. Two minority-spin bands with highest energy form the bottom of the conduction band with Sn 5*s* states. Two minority-spin bands locate across the Fermi level, forming the top of the valence band with S 3*p* states and up-shifting the VBM. In this situation, the energy difference between VBM and CBM is 1.44 eV, which is smaller than the band gap value of pure SnS_2 (1.81 eV). Thus,

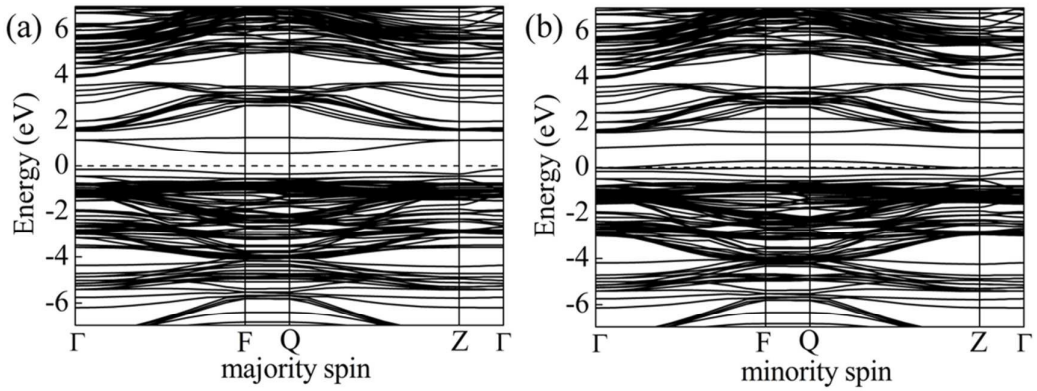

Fig. 3 Band structure of Fe-doped SnS_2 for doping concentration x = 6.25%, with (a) majority spin and (b) minority spin. The Fermi level is set to 0.

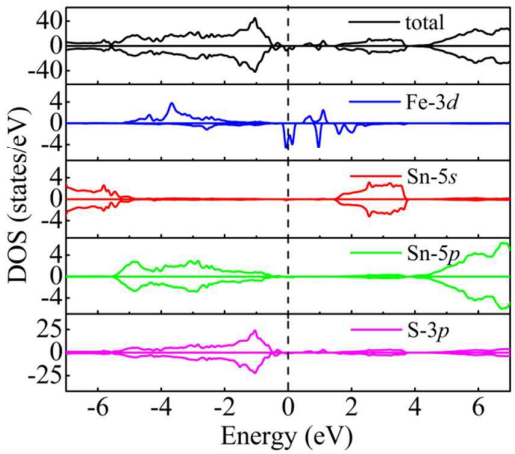

Fig. 4 TDOS and PDOS of Fe-doped SnS_2 for doping concentration x = 6.25%. The Fermi level is set to 0.

compared with pure SnS_2, it requires less energy for electron transition from the occupied states to the unoccupied states, which means the absorption edges of Fe-doped SnS_2 may occur red shift. The last one minority-spin and two majority-spin bands are in the energy range between 0.54 and 1.24 eV, which can absorb the low-energy photons, and then extend the absorption of SnS_2 into infrared region. Full detailed information will be discussed in the following sections.

As we all know, optical properties of photovoltaic absorber materials are very crucial for optoelectronic devices. The components of optical properties corresponding to parallel to the c axis (E // c) have been discussed in the present work, due to the greatest incident optical absorption coefficient along this direction. Then, the effect of Fe doping on optical properties of SnS_2 will be comprehensively studied in the following part, and the doping concentrations are varied from x = 0% to 12.50%.

Based on the quantum theory, photons absorbed and emitted are the reasons for electron transitions between occupied and unoccupied states, including single-particle excitations and plasmons. And it should also be noted that the contribution from the two-band process has been proved strictly to be zero.[36] It is necessary to calculate the dielectric function $\varepsilon(\omega)=\varepsilon_1(\omega)+i\varepsilon_2(\omega)$ to completely characterize the optical properties of bulk materials based on SnS_2.[37] The imaginary part of the dielectric function $\varepsilon_2(\omega)$ not only is related to the electronic structure of materials, but also presents the optical properties. It can be given as[38]

$$\varepsilon_2(\omega)=\left(\frac{4\pi^2e^2}{m^2\omega^2}\right)\sum_{i,j}\int\langle i|M|j\rangle^2 f_i(1-f_j)\delta(E_f-E_i-\omega)d^3k \quad (1)$$

where i and j are the initial and final states, respectively, M is the dipole matrix. f_i and E_i are the Fermi distribution function and the energy of electron in ith state respectively. The real part of the dielectric function $\varepsilon_1(\omega)$ can be evaluated from the imaginary part $\varepsilon_2(\omega)$ with Kramers-Kronig transformation.

$$\varepsilon_1(\omega)=1+\frac{2}{\pi}P\int_0^\infty\frac{\omega'\varepsilon_2(\omega')d\omega}{(\omega'^2-\omega^2)} \quad (2)$$

Then, other optical constants such as absorption coefficient $\alpha(\omega)$, reflectivity $R(\omega)$, refractivity index $n(\omega)$ and energy-loss $L(\omega)$ can be obtained from $\varepsilon_1(\omega)$ and $\varepsilon_2(\omega)$.[39]

$$\alpha(\omega)=\sqrt{2}\omega\left[\sqrt{\varepsilon_1^2(\omega)+\varepsilon_2^2(\omega)}-\varepsilon_1(\omega)\right]^{1/2} \quad (3)$$

$$R(\omega)=\left|\frac{\sqrt{\varepsilon_1(\omega)+j\varepsilon_2(\omega)}-1}{\sqrt{\varepsilon_1(\omega)+j\varepsilon_2(\omega)}+1}\right|^2 \quad (4)$$

$$n(\omega)=(1/\sqrt{2})\left[\sqrt{\varepsilon_1^2(\omega)+\varepsilon_2^2(\omega)}-\varepsilon_1(\omega)\right]^{1/2} \quad (5)$$

$$L(\omega)=\varepsilon_2(\omega)/\left[\varepsilon_1^2(\omega)+\varepsilon_2^2(\omega)\right] \quad (6)$$

The imaginary part spectra of the dielectric function for Fe-doped SnS_2 with five different doping concentrations are presented in Fig. 5(a). For pure SnS_2, we can see two primary peaks. One locates at 3.88 eV, which originates the electronic transition from the 3p orbitals of the S atom in the upper valence band to the 5s orbitals of the Sn atom in the lowest conduction band. The other locates at 7.32 eV, which originates the electronic transition from the 3p orbitals of the S atom in the valence band to the 5p orbitals of the Sn atom in the conduction band. In the case of Fe-doped SnS_2 systems, the obvious changes are that there appear new peaks in low energy region, indicating new and distinct channels for the absorption of photons with energies below the gap width of SnS_2 are obtained. The emerging peaks are at 0.29, 0.30, 0.29 and 0.42 eV for Fe doping concentrations of x = 5.56%, 6.25%, 8.33% and 12.50%, respectively, which are due to the electronic

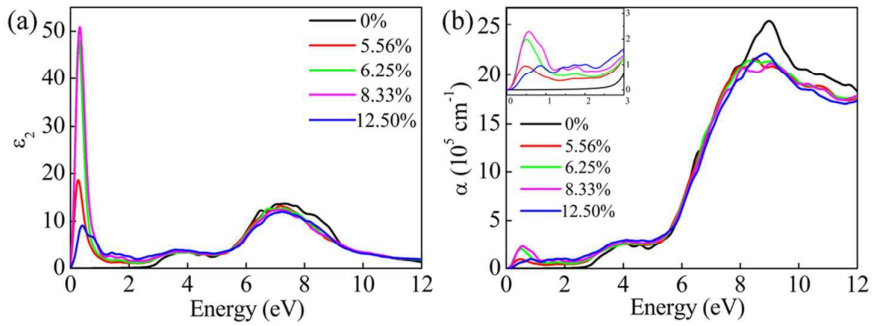

Fig. 5 (a) The imaginary part of the dielectric function and (b) the absorption coefficient spectra of $Sn_{1-x}Fe_xS_2$ (x = 0%, 5.56%, 6.25%, 8.33%, 12.50%). The inset is the enlarged view of infrared and visible light absorption spectra.

Journal Name

ARTICLE

intraband transition of the impurity Fe 3*d* states and the Sn 5*s* states in the conduction band. Besides, the emerging peaks correspond to the localized degree of the impurity bands we discussed on electronic properties above. Obviously, the intensity of emerging peaks increases with small doping concentrations (less than x = 8.33%) and decreases with heavy doping, which implies that there is a critical doping concentration for the strongest absorption in infrared region. In addition, the peaks similar to pure SnS_2 locate at around 3.59 to 4.08 eV and 7.19 to 7.27 eV. The former corresponds to the electronic transition from the S 3*p* states in the valence band to the Sn 5*s* states in the conduction band. While the later corresponds to the electronic transition from the S 3*p* states in the valence band to the Sn 5*p* states in the conduction band. What is noteworthy is that for different structure configurations of SnS_2, the shape and the strength of the curves are nearly identical in the high energy region. These characteristics imply that different doping concentrations of Fe have a significant influence on the optical properties of SnS_2 systems in low energy region, including visible and infrared region, while the effect is barely noticeable in ultraviolet region, which demonstrates that Fe-doped SnS_2 systems are more suitable for long-wavelength optoelectronic devices compared with pure SnS_2.

The absorption spectra of all the SnS_2 systems are illustrated in Fig. 5(b). From the overall trend of spectra we can see that the absorption range is very wide, and the ultraviolet region is still the main absorption part. Compared with undoped SnS_2, the absorption coefficient of Fe-doped SnS_2 in visible region increases with increasing Fe doping concentrations, which is mainly induced by the enhancement of Fe 3*d* impurity states. Meanwhile, the additional absorption part is obtained in the infrared and visible region which is below the absorption edges for Fe-doped SnS_2 systems. This phenomenon is deduced from the electronic intraband transition of the impurity Fe 3*d* states and the Sn 5*s* states in the conduction band. Chen *et al*. found the similar phenomenon when studied the Fe-doped In_2S_3.[27] Besides, the emerging peaks in low energy region will improve the utilization efficiency of sunlight in infrared region, which has a good consistency with the above discussion about the imaginary part of the dielectric function. What's more, it can also be seen from Fig. 4 that the additional Fe 3*d* states in the band gap are the main reason that the peaks emerge in low energy region. In addition, the absorption edges of Fe-doped SnS_2 systems monotonically shift to the lower energy with the increase of the Fe doping concentrations, which is mainly the result of the decrease of band gaps of Fe-doped SnS_2 systems. The phenomenon of red shift is in accordance with the above analysis of electronic structure. Therefore, the Fe doping will become a crucial factor that affects optical properties of SnS_2. And more notably, Fe-doped SnS_2 shows more efficient utilization of solar energy compared with Ti, Zn and V-doped SnS_2. In terms of the optical absorption, compared with

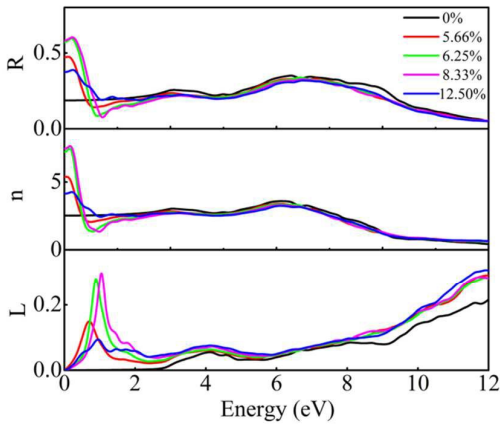

Fig. 6 (a) The reflectivity, (b) refractivity index, and (c) energy-loss spectra of $Sn_{1-x}Fe_xS_2$ (x = 0%, 5.56%, 6.25%, 8.33%, 12.50%).

undoped SnS_2, Fe-doped SnS_2 can obtain an obvious increase in the energy range of about 0 to 6.5 eV, while V, Ti and Zn-doped SnS_2 enhance the absorption efficiency of solar spectrum in the energy of about 0 to 3.8 eV, 2.0 to 6.0 eV and more than 3.4 eV, respectively.[22-24] According to the above discussion, it can be concluded that the Fe doping can make SnS_2 a potential candidate for optoelectronic devices.

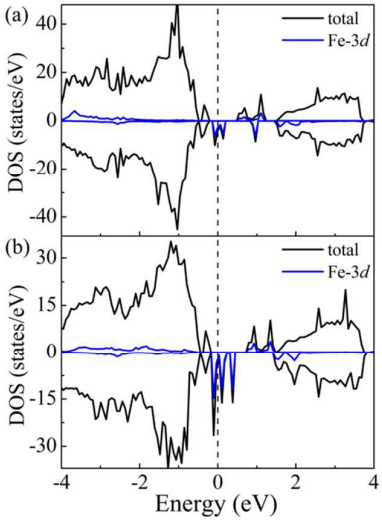

Fig. 7 The calculated DOS of Fe-doped SnS_2 for doping concentration x = 6.25% with the GGA+U method, where U = 9 eV for Sn-4*d*, (a) U = 1.7 eV and (b) U = 0 eV for Fe-3*d* are used. The Fermi level is set to 0.

Journal Name

ARTICLE

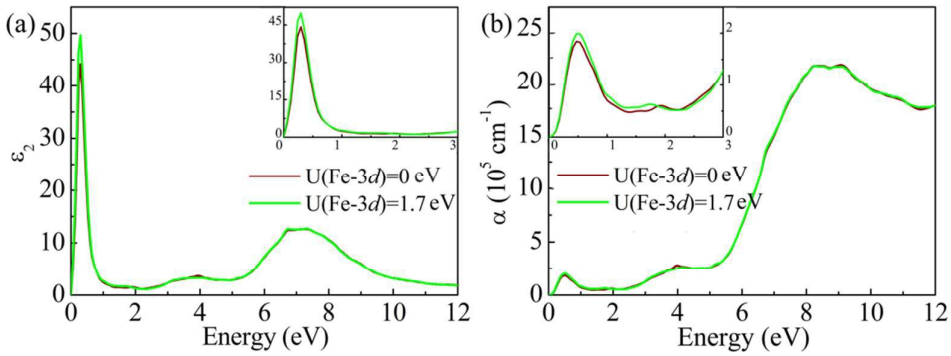

Fig. 8 (a) The calculated imaginary part of the dielectric function and (b) the absorption coefficient spectra of $Sn_{1-x}Fe_xS_2$ (x = 6.25%) with the GGA+U method, where U = 9 eV for Sn-4d, U = 1.7 and U = 0 eV for Fe-3d are used. The inset is the enlarged view of spectra in the infrared and visible region.

The reflectivity $R(\omega)$, refractivity index $n(\omega)$ and energy-loss $L(\omega)$ spectra of five different structure configurations of SnS_2 systems are presented in Fig. 6. For the Fe-doped SnS_2, the reflectivity and refractivity index enhance much in the low energy region, which mainly originates from the impurity bands near the Fermi level. Besides, both of them show the strongest peaks at around 0.2 eV and decrease abruptly in the low energy range between 0.2 and 1.2 eV. The location of reflectivity and refractivity peaks also agree with the imaginary part spectrum of dielectric function. Moreover, the energy-loss peaks at around 1.1 eV are related to the plasma oscillations where the reflectivity decreases rapidly. The above results indicate that the optical properties of Fe-doped SnS_2 can get significantly improved in the low energy region, while the effect is less obvious in the ultraviolet region.

All the above results are obtained on the basis of the GGA+U method. It is generally known that the calculated band gap depends on the U value of Hubbard model adopted in the calculations. And we have proved that the value of U adopted for Sn is in great agreement with the experimental band gap of pure SnS_2. However, the gap of Fe-doped SnS_2 may also rely on the U value for Fe. In order to explore the effect of the U value for Fe on the electronic and optical properties of Fe-doped SnS_2, the doped bulk system $Sn_{15}Fe_1S_{32}$ corresponding to 6.25% doping concentration is chosen as a reference. Besides, the DOS, the imaginary part of the dielectric function and the absorption coefficient of $Sn_{15}Fe_1S_{32}$ are calculated using the GGA+U method, where U = 9 eV for Sn-4d and U = 0 eV for Fe-3d are used. The results are presented in Fig. 7 and Fig. 8, respectively. The band gap obtained from Fig. 7(b) is 0.89 eV, which is considerably narrower than that of the doped system with the same structure corresponding to U = 9 eV for Sn-4d and U = 1.7 eV for Fe-3d. The reason is that the majority-spin intermediate states are lifted toward the CBM and then down-shift the CBM. It can be concluded from Fig. 7 that the effective Hubbard correction can lower the occupied majority spin states and raise the unoccupied minority spin states. Namely, the energy states of the intermediate states of Fe-doped SnS_2 are largely determined by the U value for Fe. While the U value for Fe has little effect on the optical properties of Fe-doped SnS_2. It can be seen from Fig. 8 that the similar results are obtained with U = 0 and U = 1.7 eV for Fe-3d, which indicates that the results of the GGA+U (U = 9 eV for Sn-4d and U = 1.7 eV for Fe-3d) method can qualitatively reflect the properties of Fe-doped SnS_2 systems.

4. Conclusion

In conclusion, we have systematically studied the electronic structure and optical properties of Fe-doped SnS_2 systems in five different structure configurations with the method of first-principle calculations. The electronic structures imply Fe-doped SnS_2 systems are half-metal due to the shift of Fermi level from the VBM into valence band. The band gap of Fe-doped SnS_2 can be decreased from 1.81 to 1.44 eV when the Fe doping concentration is x = 6.25%. Moreover, the absorption edges of Fe-doped SnS_2 systems show red shift. The absorption coefficient in visible region increases monotonically with increasing Fe doping concentrations. These characteristics indicate that Fe-doped SnS_2 system is a potential candidate for optoelectronic devices. In addition, the electronic intraband transition of the impurity Fe 3d states and the Sn 5s states in the conduction band broadens the sunlight absorption into the infrared region. The intensity of emerging peaks in infrared

region increases with small doping concentrations (less than x = 8.33%) and decreases with heavy doping. Our calculations provide adequate proofs for effective utilization of solar energy, especially in low energy region. These results not only contribute to designing novel solar cell based on SnS_2 host, but also promote the further experimental studies.

Acknowledgements

This work was supported by the National Natural Science Foundation of China (51572190) and (11247224), and the supercomputing resources were supported by High Performance Computing Center of Tianjin University, China.

Notes and references

[a]*Department of Applied Physics, Tianjin Key Laboratory of Low Dimensional Materials Physics and Preparing Technology, Faculty of Science, Tianjin University, Tianjin 300072, People's Republic of China.*
[b]*College of Chemical Engineering, North China University of Science and Technology, Tangshan 063009, People's Republic of China.*
E-mail:pingwu@tju.edu.cn (P. Wu).; Tel: +86 02227408599

1 M. Grätzel, *Nature*, 2001, **414**, 338-344.
2 D. E. Carlson and C. R. Wronski, *Appl. Phys. Lett*., 1976, **28**, 671.
3 C. Candelise, M. Winskel and R. Gross, *Prog. Photovoltaics*, 2012, **20**, 816.
4 M. A. Green, *Prog. Photovoltaics*, 2001, **9**, 123.
5 S. Lany and A. Zunger, *Phy., Rev. B*, 2005,**72**, 035215.
6 S. Kumar, M. Gradzielskic and S. K. Mehta, *RSC Adv.*, 2013, **3**, 2662-2676.
7 Y. H. Huang, Z. Q. Zhang, F. Ma, P. K. Chu, C. P. Dong and X. M. Wei, *Comput. Mater. Sci.*, 2015, **101**, 1-7.
8 A. Kumar and P. K. Ahluwalia, *Mater. Chem. Phys.*, 2012, **135**, 755-761.
9 P. Lazić, R. Armiento, F. W. Herbert, R. Chakraborty, R. Sun, M. K. Y. Chan, K. Hartman, T. Buonassisi, B. Yildiz and G. Ceder, *J. Phys.: Condens. Matter*, 2013, **25**, 465801.
10 H. S. Lee, S. -W. Min, Y. -G. Chang, M. K. Park, T. Nam, H. Kim, J. H. Kim, S. Ryu and S. Im, *Nano Lett*., 2012, **12**, 3695-3700.
11 R. J. Wei, J. C. Hu, T. F. Zhou, X. L. Zhou, J. X. Liu and J. L. Li, *Acta Mater*., 2014, **66**, 163.
12 D. L. Greenaway and R. Nitsche, *J. Phys. Chem. Solids*, 1965, **26**, 1445.
13 R. Bacewicz, B. Palosz, W. Palosz and S. Gierlotka, *Solid State Commun.*, 1985, **54**, 283.
14 H. X. Zhong, G. Z. Yang, H. W. Song, Q. Y. Liao, H. Cui, P. K. Shen and C. X. Wang, *J. Phys. Chem. C*, 2012, **116**, 9319.
15 Y. C. Zhang, Z. N. Du, S. Y. Li and M. Zhang, *Appl. Catal. B*, 2010, **95**, 153-159.
16 L. A. Burton and A. Walsh, *J. Phys. Chem. C*, 2012, **116**, 24262.
17 J. L. Gole, J. D. Stout, C. Burda, Y. Lou and X. Chen, *J. Phys. Chem. B*, 2004, **108**, 1230.
18 C. G. Van de Walle and J. Neugebauer, *J. Appl. Phys*., 2004, **95**, 3851.
19 R. Etefagh, N. Shahtahmasebi and M. Karimipour, *Bull. Mater. Sci*., 2013, **36**, 411-416.
20 O. A. Yassin, A. A. Abdelaziz and A. Y. Jaber, *Mater. Sci. Semicond. Process*., 2015, **38**, 81-86.
21 M. J. Powell, *J. Phys. C: Solid State Phys*., 1977, **10**, 2967.
22 C. Xia, J. An, T. Wang, S. Wei and Y. Jia, *Acta Mater*., 2014, **72**, 223-228.
23 G. Kiruthigaa, C. Manoharan, C. Raju, S. Dhanapandian and V. Thanikachalam, *Mater. Sci. Semicond. Process*., 2014, **26**, 533-539.
24 P. Wahnon, J. C. Conesa, P. Palacios, R. Lucena, I. Aguilera, Y. Seminovski and F. Fresno, *Phys. Chem. Chem. Phys*., 2011, **13**, 20401-20407.
25 Y. Seminovski, P. Palacios and P. Wahnón, *J. Phys.: Condens. Matter*, 2014, **26**, 395501.
26 A. Rohrbach, J. Hafner and G. Kresse, *J. Phys.: Condens. Matter*, 2003, **15**, 979.
27 P. Chen, H. Chen, M. Qin, C. Yang, W. Zhao and Y. Liu, *J. Appl. Phys*., 2013, **113**, 213509.
28 P. E. Blöchl, *Phys. Rev. B*, 1994, **50**, 17953.
29 J. P. Perdew, K. Burke and M. Ernzerhof, *Phys. Rev. Lett*., 1996, **77**, 3865-3868.
30 H. J. Monkhorst and J. D. Pack, *Phys. Rev. B*, 1976, **13**, 5188.
31 S. J. Grimme, *Comput. Chem*., 2006, **85**, 1787.
32 A. J. Cohen, P. Mori-Sanchez and W. T. Yang, *Chem. Rev*., 2012, **112**, 289.
33 S. L. Dudarev, G. A. Botton, S. Y. Savrasov, C. J. Humphreys and A. P. Sutton, *Phys. Rev. B*, 1998, **57**, 1505.
34 C. X. Xia, Y. T. Peng, H. Zhang, T. X. Wang, S. Y. Wei and Y. Jia, *Phys. Chem. Chem. Phys*., 2014, **16**, 19674.
35 S. K. Arora, D. H. Patel and M. K. Agarwal, *Cryst. Res. Technol*., 1993, **28**, 623.
36 B. B. Zhang, M. H. Lee, Z. H. Yang, Q. Jing, S. L. Pan, M. Zhang, H. P. Wu, X. Su and C. S. Li, *Appl. Phys. Lett*., 2015, **106**, 031906.
37 R. Chowdhury, S. Adhikari and P. Rees, *Physica B*, 2010, **405**, 4763.
38 C. M. I. Okoye, *J. Phys.: Condens. Matter*, 2003, **15**, 5945.
39 L. Y. Li, W. H. Wang, H. L, X. D. Liu, Q. G. Song and S. W. Ren, *J. Phys. Chem. C*, 2009, **113**, 8460-8464.

The Fe doping can increase the visible absorption of SnS_2 and extend the absorption into the infrared region.

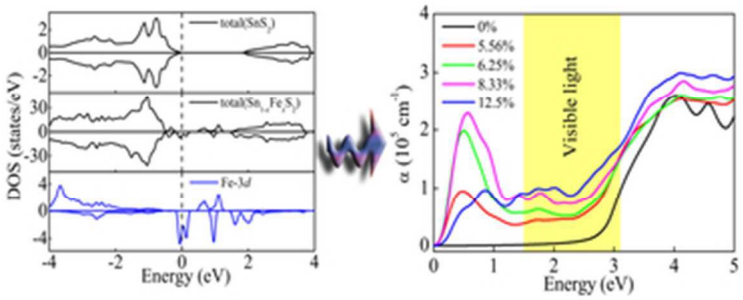

32x12mm (300 x 300 DPI)